Editors' Suggestion | Featured in Physics

Probing Interfacial Water Dissociation at the Nanoscale with a Quantum Sensor

Wentian Zheng,[1,*] Ke Bian,[1,2,*,†] Jiyu Xu,[3,4,*] Xiakun Chen,[1] Shichen Zhang,[1] Rainer Stöhr,[5,6] Andrej Denisenko,[5,6] Jörg Wrachtrup,[5,6] Sheng Meng,[3,4,‡] and Ying Jiang[1,2,7,8,§]

[1]*International Center for Quantum Materials, School of Physics, Peking University, Beijing, 100871, People's Republic of China*
[2]*Interdisciplinary Institute of Light-Element Quantum Materials and Research Center for Light-Element Advanced Materials, Peking University, Beijing, 100871, People's Republic of China*
[3]*Beijing National Laboratory for Condensed Matter Physics and Institute of Physics, Chinese Academy of Sciences, Beijing, 100190, People's Republic of China*
[4]*Songshan Lake Materials Laboratory, Dongguan, Guangdong, 523808, People's Republic of China*
[5]*3rd Institute of Physics, University of Stuttgart and Institute for Quantum Science and Technology (IQST), Stuttgart, 70569, Germany*
[6]*Max Planck Institute for Solid State Research, Stuttgart, 70569, Germany*
[7]*Collaborative Innovation Center of Quantum Matter, Beijing, 100871, People's Republic of China*
[8]*New Cornerstone Science Laboratory, Peking University, Beijing 100871, People's Republic of China*

(Received 31 January 2025; accepted 15 September 2025; published 10 November 2025)

Controlling and monitoring interfacial chemical reactions is crucial for electrochemistry and photochemistry. Here, we developed a new type of interface-sensitive magnetic resonance technique by combining qPlus-based scanning probe microscopy (SPM) and quantum sensing based on a single nitrogen-vacancy center near the surface of a diamond. Using this technique, we investigated water dissociation at the hydrophilic diamond surface and monitored its elementary steps, including electron transfer, bond breaking, as well as water and hydrogen diffusion. The SPM tip was used to locally inject electrons into the interfacial water, and the resulting hydrated electrons ($e^-_{(aq)}$) were found to have specific configurations at the interface with a hyperfine interaction of about 28 MHz, which agrees with density-functional theory calculations. We observed that $e^-_{(aq)}$ can induce water dissociation and the reaction product hydroxides diffuse ~2.3 times faster than water molecules. The diffusion coefficients of water and the reaction product hydroxides at the interface are about 3 orders of magnitude smaller than those in the bulk phase, but their ratio almost remain the same. These results show that the combination of SPM and quantum sensing provides a new platform to reveal the detailed electronic and nuclear processes of interfacial chemical reactions with nanometer resolution.

DOI: 10.1103/gpcy-lnc2

Controlling and monitoring the elementary steps of interfacial chemical reactions from a microscopic view is highly demanding as it is essential both for revealing the underlying mechanisms and promoting the efficiency of various processes in heterogeneous catalysis. However, achieving this goal presents a great challenge, requiring an interface-sensitive technique with the ability of chemical identification. Surface-enhanced Raman spectroscopy [1] and sum-frequency generation spectroscopy [2,3] can be highly interface-sensitive but suffer from spatial averaging. Accordingly, scanning probe microscopy (SPM) stands out due to its exceptional capability for manipulating and investigating chemical reactions even at the single-molecule level [4]. SPM-based techniques such as inelastic electron tunneling spectroscopy [5,6] and tip-enhanced Raman spectroscopy [7,8] can recognize different isotopes and chemical bonds at the nano and atomic scale. However, all these interface-sensitive techniques rely on the vibration modes of chemical bonds that have a large cross section of inelastic scattering with the tunneling electrons or photons, thus limiting their applications in molecules with specific electronic structures or symmetries. In addition, those vibrational techniques cannot directly detect unpaired electrons, such as radicals or reducing agents, in the intermediate products, that play an important role in elucidating the cycles of chemical reactions.

Nuclear magnetic resonance (NMR) and electron spin resonance (ESR) are widely used in analyzing the elementary components of molecules as well as chemical reactions, but conventionally, they are not interface-sensitive. Recently, NMR and ESR have been successfully realized with nanoscale resolution. The technique is based on the detection by the nitrogen-vacancy (NV) centers in diamonds [9–13], achieving high sensitivity up to single

*These authors contributed equally to this work.
†Contact author: bian.k@pku.edu.cn
‡Contact author: smeng@iphy.ac.cn
§Contact author: yjiang@pku.edu.cn

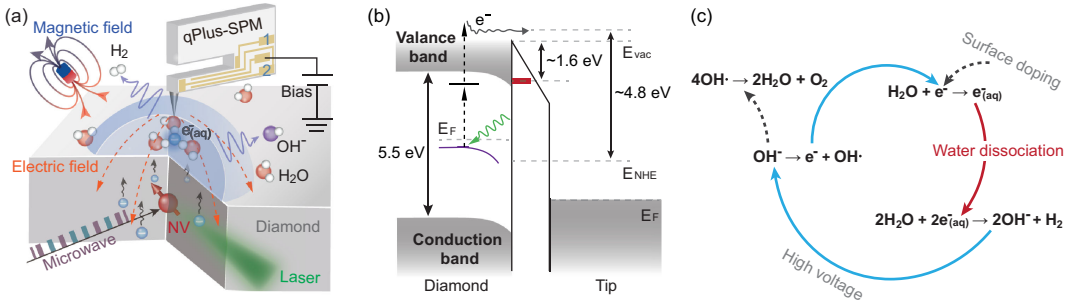

FIG. 1. (a) A sharp conductive tip was approached to the diamond surface, then pulled up the electrons (blue sphere) from the diamond and controlled the H_2O dissociation. A shallow NV center with nanoscale detection volume (translucent hemisphere) was used to apply the nanoscale ESR and NMR and identify the intermediate and final product of the H_2O dissociations. Atomic force microscope signals are labeled as 1 and 2. (b) Energy level showing the mechanism of surface doping by the strong local electric field of the tip. With a 532-nm laser (green wave), the electrons at the donor level (purple line) were activated into the conduction band, pulled up to the surface, and doped into the hydration layer with a large reduction potential. The electrochemical reaction potential for $e^- + H_2O \rightarrow e^-_{(aq)}$ is marked by a red line. E_F, E_{vac}, and E_{NHE} denote the Fermi level, vacuum level, and absolute energy of normal hydrogen electrode, respectively. (c) The schematic shows the process of H_2O dissociation, where the reaction paths of H_2O and its dissociated products under different tip biases are presented.

electron and nuclear spins through advanced quantum sensing techniques [14–17]. Meanwhile, benefitting from the atomic size and the dipolar interactions [10] (falling as $\sim 1/r^3$), a shallow NV center brought in proximity to the diamond surface allows for probing the chemical shift of various species [10,12,18] within a detection volume of only several nanometers at ambient conditions. However, it has not been possible to resolve the elementary steps of chemical reactions by NVs due to the lack of capability to locally trigger and control chemical reactions. One promising way to solve this problem is to use the tips of a scanning probe microscope.

Here, we demonstrated the nanoscale control and characterization of chemical reactions using our homemade scanning quantum sensing microscope under ambient conditions [19] [see Supplemental Material (SM) [20]], which combined both qPlus-based SPM and NV-based quantum sensing. We chose to investigate water (H_2O) dissociation at the solid-water interface as it is an exemplary reaction of great importance in electrochemistry and photochemistry. In this system, a sharp conductive SPM tip with a strong local electric field was applied to trigger the H_2O dissociation in the hydration layers at the nanoscale on the diamond surface, where the electrons from the defects of the diamond were photoactivated and pulled out to the diamond surface [51]. Simultaneously, the shallow NV center beneath the diamond surface served as a sensor to monitor the reaction processes, including the electron transfer, bond breaking, and hydrogen diffusion at the interface. After injecting the electrons into the adsorbed hydration layers, we detected the hydrated electrons ($e^-_{(aq)}$) [52,53] through double electron-electron resonance (DEER) [54] and their successive products of hydroxides (OH^-) or radicals ($OH\cdot$) through nanoscale NMR. These results showed that the combination of SPM and shallow NV centers opens up new possibilities to investigate unprecedentedly detailed processes of interfacial chemical reactions with nanometer resolution.

Figure 1(a) shows the schematics of the experimental setup. A diamond with an oxygen-terminated hydrophilic surface after acid treatments was placed under the tip of the homemade scanning quantum sensing microscope. It has been confirmed that the hydration layer exists on an oxygen-terminated diamond surface at ambient conditions [11,13,18]. Shallow NV centers were created by overgrowing the boron-doped sacrifice layers before ion implantations (see SM [20]), leading to high-quality NV centers capable of nanoscale NMR [55]. The SPM tip was assembled on a qPlus-type force sensor [56], which can work stably even under aqueous conditions [57]. A magnetic field was applied along the axis of the NV center, and the laser and microwave pulses were used to read out and control the quantum state of NV. A sharp tungsten tip with a large positive bias voltage was used to locally dope the surface hydration layers near the shallow NV centers [51,58], where the tip bias was well isolated from the atomic force microscope electrodes (see SM and Fig. S1 [20]). Because of the small oscillating amplitudes of the qPlus sensor (hundreds of pm), the biased tip would bring negligible electric noise to shallow NV centers during the experiments [51]. In our case, the tip was not coated with an insulating layer, since the diamond is an insulator, and no reference or counter electrodes were applied as in an electrochemical cell (see SM [20]) [59].

The energy level of the NV center lies 2.9 eV above the valence band within the band gap (5.5 eV) of a diamond [60]. For an oxygen-terminated diamond surface, the vacuum level is ~1.7 eV above the bottom of the conduction band [61]. When the NV was illuminated by a 532-nm (corresponding to 2.33 eV) laser, the unpaired electrons of the defects (donors) introduced during the NV growth were ionized into the conduction band through a two-photon

process [Fig. 1(b)] [51]. With the assistance of the tip's strong local electric field, the activated electrons can be pulled onto the diamond surface and transferred to the hydration layers with a large reduction potential (~ -4.8 eV) versus the normal hydrogen electrode, which lies ~4.4 eV below the vacuum level [62]. In this case, $e^-_{(aq)}$ was produced through $e^- + H_2O \rightarrow e^-_{(aq)}$ [62] and induced a series of chemical processes as depicted in Fig. 1(c). Redox reaction can easily occur owing to the strong reducibility of $e^-_{(aq)}$ [53,63,64]: $2H_2O + 2e^-_{(aq)} \rightarrow H_2 + 2OH^-$. In this case, the accumulation of OH^- on the diamond surface induced the upward band bending and depleted the NV^- (without specific statements, NV represents NV^- for convenience in this Letter) to a nonfluorescent NV^+ state, which we denoted as the benchmark of surface doping through the SPM tip (see SM and Fig. S2 [20]) [51]. As the tip's voltage further increased, the OH^- can dissociate into a free electron and a hydroxyl radical (OH·): $OH^- \rightarrow OH\cdot + e^-$, under a strong electric field at the level of V/nm [65,66]. In this case, the electrons were released back into the surrounding aqueous environment and produced the $e^-_{(aq)}$ again. At the same time, the product of OH· was unstable and supposed to produce hydrogen peroxide [65]: $2OH\cdot \rightarrow H_2O_2$, and further dissociated into H_2O and oxygen: $2H_2O_2 \rightarrow 2H_2O + O_2$.

The tungsten tip can be positioned over the NV center through the quenching effect [Fig. 2(a)] [67]. By continuously monitoring the NV's fluorescence when scanning the tip around, a drop in fluorescence occurred when the tip was close to the NV center. Because of the sharpness of the SPM tip, these interactions can, in principle, be controlled with a nanometer spatial resolution, which is determined by the tip's electric-field distribution (Figs. S3 and S4 [20]). Here, we used the charge state of NV as the electric-field sensor. We mapped the charge state transition [51] of NV under different tip biases [Fig. 2(b)]. First, nonfluorescent NV^+ was generated due to the accumulated negative charges such as OH^-, as a result of tip-induced H_2O dissociation. Then, a positively biased tip scanned around the same NV and locally recovered its fluorescence through the tip-induced band bending effect. The qPlus signal was also monitored simultaneously, albeit showing no obvious features that correlate with the charge accumulation after H_2O dissociation because the quality factor and force sensitivity of qPlus are limited under ambient conditions.

To investigate the unpaired electrons such as $e^-_{(aq)}$ caused by the surface doping, we applied the NV-based DEER spectroscopy [54], as illustrated in the upper panel of Fig. 2(c). A spin-echo sequence (marked in blue) was applied to decouple the NV from the unwanted magnetic noise in the environment, where an extra microwave π pulse (marked in orange) was used to selectively flip the target electron spins. When the frequency of the extra π pulse was resonant with the electron spins, the measured fluorescence of the NV after the DEER sequence was

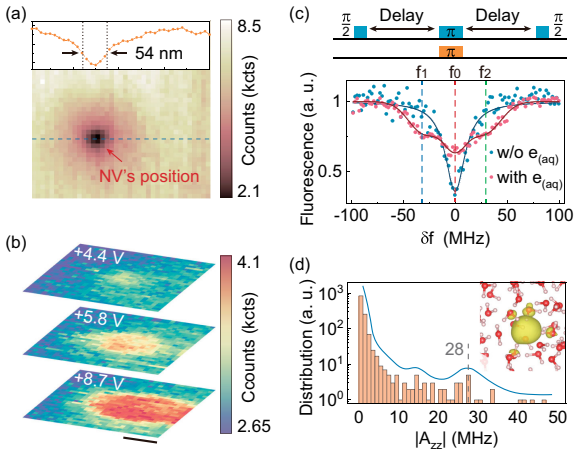

FIG. 2. (a) Positioning the tip over an NV center through the quenching effect. The line profile shows a positioning accuracy of 54 nm. (b) Charge state transition mappings of a single NV at different tip biases. The bright region shrinks with the decreased tip bias, indicating the decreased field strength of the SPM tip. Data were acquired with a laser power of 15 μW. Scale bar: 50 nm. (c) DEER of a shallow NV center with (red curve) and without (blue curve) $e^-_{(aq)}$. With $e^-_{(aq)}$, $f_0 = 1.544$ GHz remains, and two shoulders appear at $f_1 = 1.513$ GHz and $f_2 = 1.574$ GHz. The frequency is shifted according to: $\delta f = f - f_0$ for clarity. The delay time was fixed at 10 μs. (d) Distribution of the calculated $|A_{zz}|$ between protons in H_2O and $e^-_{(aq)}$, showing a maximum of around 28 MHz. The blue curve is used to guide the eye. Inset: one of the simulated structures of $e^-_{(aq)}$ caged by 64 H_2O molecules.

reduced due to decoherence caused by the magnetic noise of these electron spins. The blue curve in Fig. 2(c) shows the typical DEER spectrum of a shallow NV center, with a resonance peak (f_0) consistent with the Larmor frequency of the electron spins of $g = 2$ (1.544 GHz under a magnetic field of ~550 Gauss), which is attributed to the unpaired electrons of the near-surface defects in diamond [54,68]. After positioning a tip with a large positive bias (+45 V) around the shallow NV, the DEER spectrum shows an overall broadened feature (red curve) with two shoulders centered around 1.513 and 1.574 GHz (marked by f_1 and f_2), which indicates an extra interaction such as the hyperfine interaction between the nuclei spins and these unpaired near-surface electrons. To confirm that the $e^-_{(aq)}$ were produced by pulling the electrons from the diamond defects by the tip, we also applied the DEER under various bias voltages (see SM and Fig. S5 [20]).

Figure 2(d) shows one representative hydrated configuration of $e^-_{(aq)}$ in bulk water sampled by *ab initio* molecular dynamics (AIMD) simulations and the calculated hyperfine interaction strength A_{zz} between the protons and $e^-_{(aq)}$ of ten representative hydrated configurations by density-functional theory in the absence of an external magnetic field (see SM [20]). It can be seen that there is a slight preference in the distribution of $|A_{zz}|$ of around 28 MHz, which is

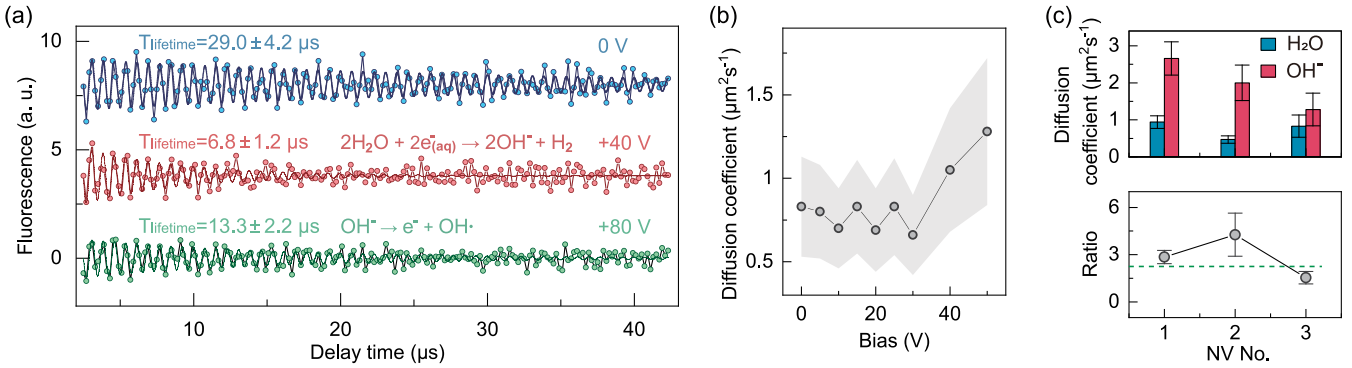

FIG. 3. (a) Correlation data using XY8-4 of a single NV under different tip biases. The oscillation is consistent with the protons' Larmor frequency, with a decayed envelope caused by the diffusion of protons in H_2O and OH^-. The fitting of $T_{lifetime}$ was described in SM [20]. (b) Diffusion coefficients of protons at different tip biases, the shaded areas denote the experimental error. (c) Diffusion coefficients of protons in H_2O and OH^- measured by three NVs at the diamond surface. The ratio of proton diffusion coefficients in interfacial H_2O and OH^- is consistent with that in the bulk phase (the dashed line). This proves that a correlation measurement can be used to identify the OH^- at the nanoscale.

attributed to the protons within the radius of gyration of $e^-_{(aq)}$, quantitatively consistent with the shoulder peaks shown in Fig. 2(c). It is worth noting that the water structure at the hydrophilic diamond surface should be more ordered than the bulk phase [1,69], which may lead to more specific hydrated configurations of $e^-_{(aq)}$ and pronounced peak splitting in DEER measurements.

The products of H_2O dissociation, OH^-, have no net electron spin magnetic moment, thus showing no signals in the NV-based ESR spectroscopy. However, we can probe the diffusion dynamics of OH^- by the nanoscale NMR based on the correlation spectrum [70,71], which resembles the nuclear free induction decay in conventional NMR (see SM and Fig. S6 [20]). Figure 3(a) shows the correlation spectra of a shallow NV with and without surface electron doping. The period of the oscillation is consistent with the proton's Larmor frequency (∼1.30 MHz) under a magnetic field of 305 Gauss, which can be further confirmed by the power density spectrum through fast Fourier transform (Fig. S7 [20]). Since the free induction decay of proton spins in liquid water or adsorbed hydrocarbons is in the range of 0.1–10 ms [12,72,73], the decayed envelope of only several tens of μs should result from the limited lifetime of the diffusive protons in H_2O or OH^- within the nanometer-size detection volume of NV center [71] (Fig. S7 [20]) at room temperature. With the measured lifetime, we can quantitatively calculate the diffusion coefficient of protons in H_2O or OH^- at the diamond surface (see SM [20]) [12,74]. According to the Grotthuss mechanism, OH^- in water can diffuse through the hydrogen-bonding network by repetitively breaking and reforming O—H bonds between neighboring H_2O molecules, with a diffusion coefficient ∼2.3 times that of H_2O [75,76]. Therefore, at the high concentration of OH^-, the measured coefficient of the protons should be dominated by the diffusion of OH^-.

After heavily doping the surface around the NV center, we found that the lifetime of protons decreased from 29.0 (blue curve) to 6.8 μs (red curve), indicating an enhanced proton diffusivity compared to that before doping [Fig. 3(a)]. Correspondingly, the power density spectrum (Fig. S7 [20]) gives a broadening of the Lorentz linewidth from 18.3 to 45.5 kHz. These results imply the existence of OH^- as a result of tip-induced H_2O dissociation. Figure 3(b) shows that the measured diffusion coefficients of protons increased at the larger tip bias, indicating the increased concentration of OH^- at the interface. Figure 3(c) shows the measured proton diffusion coefficients before (dominated by H_2O) and after (dominated by OH^-) doping the diamond surface by three NVs. Interestingly, the ratio of proton diffusion coefficients in H_2O and OH^- at the diamond surface is consistent with that in the bulk phase [denoted by the dashed line in the lower panel of Fig. 3(c)] [75,76]. The faster diffusion of OH^- relative to H_2O was also confirmed by the AIMD simulations (see SM and Fig. S8 [20]). It is worth noting that the diffusion coefficients of protons we observed were 3 orders of magnitude smaller than those in bulk water [76], possibly resulting from the oxygen termination on the hydrophilic surface in our case. The suppressed proton transfer at the interface was also confirmed by the AIMD simulations (Fig. S9 [20]).

Furthermore, the lifetime of proton spins rises to 13.3 μs under a larger bias voltage of +80 V [green curve in Fig. 3(a)]. This is attributed to the ionization of OH^- into a hydroxyl radical OH· and a free electron, which again becomes $e^-_{(aq)}$. The ionization of OH^- requires a large electric field at the level of V/nm [66], which is achievable for the sharp tungsten tip used in our experiments [51]. Such a process could decrease the concentration of OH^- and suppress the proton transfer within the hydrogen bond network of H_2O, leading to a narrowing of the NMR resonant peak (Fig. S7 [20]).

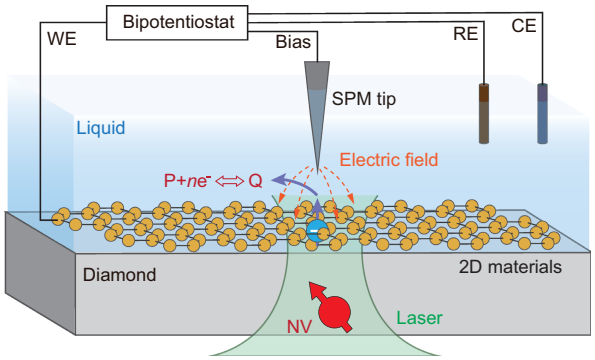

FIG. 4. The schematic shows the proposed application of combining qPlus-SPM and NV-based quantum sensing to control and investigating the unprecedentedly detailed processes of chemical reactions at the solid-liquid interface, such as in electrochemistry and photochemistry, with nanoscale resolution. Within a liquid cell, various 2D materials can be used as a model interface. The SPM tip can not only characterize the active sites but also trigger the interfacial interactions ($P + ne^- \Leftrightarrow Q$, where P and Q represent the reactants and products, respectively) by injecting high-energy electrons (denoted by the purple arrows) with high accuracy either through tunneled electrons from a conductive surface or photoactivated electrons from an insulating surface. Meanwhile, the NV-based nanoscale ESR or NMR is used to monitor the electron transfer in each reaction step, to identify the reaction (intermediate) products, and to analyze the diffusion dynamics of the products and solvents. WE, RE, and CE denote the working electrode, reference electrode, and counter electrode in the future application of electrochemistry.

To further confirm the existence of OH^- after H_2O dissociation, we performed a voltammetry measurement [59] on the diamond surface with evaporated electrodes and observed the features of electrochemical etching (see SM, Figs. S9 and S11 [20]). To confirm that the protons measured by the NV come from the H_2O instead of the hydrocarbons from the atmosphere, we applied the nanoscale NMR measurements on the hydrophobic diamond surface and barely found the signal of proton spins (see SM, Figs. S12, and S13 [20]). The hydrophobicity of the diamond surface was also confirmed by the dissipation measurements based on the qPlus sensor (see SM and Fig. S14 [20]).

Our technique opens up new possibilities for probing and manipulating elementary steps of chemical reactions at different liquid-solid interfaces, such as in electrochemistry and photochemistry. For example, as sketched in Fig. 4, within a liquid cell, instead of the hydrophilic diamond surface in this Letter, various 2D materials can be transferred onto the diamond surface and used as a model liquid-solid interface to investigate the chemical reactions. In this case, the SPM tip can be used as a nanoscopic handle to locally trigger the interfacial reactions by injecting high-energy electrons in a well-controlled manner. Meanwhile, the NV-based nanoscale ESR and NMR spectroscopies are employed to monitor the electron transfer in each reaction step, to identify the reaction (intermediate) products, and to analyze the diffusion dynamics of the products and solvents.

Acknowledgments—We are thankful for the financial support from the National Key R&D Program under Grant No. 2021YFA1400500, the Program under Grant No. 2023ZD0301300, and the National Natural Science Foundation of China under Grants No. 11888101, No. 21725302, No. 12474160, No. U22A20260, and No. 12250001, the Strategic Priority Research Program of the Chinese Academy of Sciences under Grant No. XDB28000000, and the Beijing Municipal Science and Technology Commission under Grant No. Z231100006623009. W. Z. acknowledges the China Postdoctoral Science Foundation under Grant No. 2022M710235. Y. J. acknowledges the New Cornerstone Science Foundation through the New Cornerstone Investigator Program and the XPLORER PRIZE, and the Beijing Outstanding Young Scientist Program under Grant No. JWZQ20240101002. J. X. and S. M. acknowledge financial support from the National Natural Science Foundation of China under Grants No. 12204513, No. 12025407, and No. 11934003, the Ministry of Science and Technology (No. 2021YFA1400201), Chinese Academy of Sciences (No. XDB33030100 and No. YSBR047), and Guangdong Basic and Applied Basic Research Foundation under Grant No. 2023B1515120042. R. S., A. D., and J. W. acknowledge the BMBF via Clusters4Future: QSens and the DFG under Grants No. FOR 2724, No. GRK 2642, and No. WR 28/34-1.

Data availability—The data that support the findings of this Letter are not publicly available upon publication because it is not technically feasible and/or the cost of preparing, depositing, and hosting the data would be prohibitive within the terms of this research project. The data are available from the authors upon reasonable request.

[1] Y. H. Wang, S. S. Zheng, W. M. Yang, R. Y. Zhou, Q. F. He, P. Radjenovic, J. C. Dong, S. N. Li, J. X. Zheng, Z. L. Yang, G. Attard, F. Pan, Z. Q. Tian, and J. F. Li, Nature (London) **600**, 81 (2021).
[2] M. Sovago, R. K. Campen, G. W. H. Wurpel, M. Müller, H. J. Bakker, and M. Bonn, Phys. Rev. Lett. **100**, 173901 (2008).
[3] Y. Xu, Y. B. Ma, F. Gu, S. S. Yang, and C. S. Tian, Nature (London) **621**, 506 (2023).
[4] K. Bian, C. Gerber, A. J. Heinrich, J. D. Muller, S. Scheuring, and Y. Jiang, Nat. Rev. Methods Primers **1**, 36 (2021).
[5] W. Ho, J. Chem. Phys. **117**, 11033 (2002).
[6] J. Guo, J. T. Lu, Y. X. Feng, J. Chen, J. B. Peng, Z. R. Lin, X. Z. Meng, Z. C. Wang, X. Z. Li, E. G. Wang, and Y. Jiang, Science **352**, 321 (2016).

[7] R. Zhang, Y. Zhang, Z. C. Dong, S. Jiang, C. Zhang, L. G. Chen, L. Zhang, Y. Liao, J. Aizpurua, Y. Luo, J. L. Yang, and J. G. Hou, Nature (London) **498**, 82 (2013).

[8] J. H. Zhong, X. Jin, L. Y. Meng, X. Wang, H. S. Su, Z. L. Yang, C. T. Williams, and B. Ren, Nat. Nanotechnol. **12**, 132 (2017).

[9] F. Z. Shi, Q. Zhang, P. F. Wang, H. B. Sun, J. R. Wang, X. Rong, M. Chen, C. Y. Ju, F. Reinhard, H. W. Chen, J. Wrachtrup, J. F. Wang, and J. F. Du, Science **347**, 1135 (2015).

[10] T. Staudacher, F. Shi, S. Pezzagna, J. Meijer, J. Du, C. A. Meriles, F. Reinhard, and J. Wrachtrup, Science **339**, 561 (2013).

[11] D. Rugar, H. J. Mamin, M. H. Sherwood, M. Kim, C. T. Rettner, K. Ohno, and D. D. Awschalom, Nat. Nanotechnol. **10**, 120 (2015).

[12] N. Aslam, M. Pfender, P. Neumann, R. Reuter, A. Zappe, F. F. de Oliveira, A. Denisenko, H. Sumiya, S. Onoda, J. Isoya, and J. Wrachtrup, Science **357**, 67 (2017).

[13] I. Lovchinsky, J. D. Sanchez-Yamagishi, E. K. Urbach, S. Choi, S. Fang, T. I. Andersen, K. Watanabe, T. Taniguchi, A. Bylinskii, E. Kaxiras, P. Kim, H. Park, and M. D. Lukin, Science **355**, 503 (2017).

[14] T. H. Taminiau, J. J. T. Wagenaar, T. Van der Sar, F. Jelezko, V. V. Dobrovitski, and R. Hanson, Phys. Rev. Lett. **109**, 137602 (2012).

[15] M. S. Grinolds, S. Hong, P. Maletinsky, L. Luan, M. D. Lukin, R. L. Walsworth, and A. Yacoby, Nat. Phys. **9**, 215 (2013).

[16] C. L. Degen, F. Reinhard, and P. Cappellaro, Rev. Mod. Phys. **89**, 035002 (2017).

[17] J. F. Du, F. Z. Shi, X. Kong, F. Jelezko, and J. Wrachtrup, Rev. Mod. Phys. **96**, 025001 (2024).

[18] S. J. DeVience, L. M. Pham, I. Lovchinsky, A. O. Sushkov, N. Bar-Gill, C. Belthangady, F. Casola, M. Corbett, H. L. Zhang, M. Lukin, H. Park, A. Yacoby, and R. L. Walsworth, Nat. Nanotechnol. **10**, 129 (2015).

[19] K. Bian, W. T. Zheng, X. K. Chen, S. C. Zhang, R. Stöhr, A. Denisenko, S. Yang, J. Wrachtrup, and Y. Jiang, Rev. Sci. Instrum. **95**, 053707 (2024).

[20] See Supplemental Material at http://link.aps.org/supplemental/10.1103/gpcy-lnc2 for additional experimental data and theoretical calculation, which includes Refs. [21–50].

[21] J. H. K. Pfisterer, Y. C. Liang, O. Schneider, and A. S. Bandarenka, Nature (London) **549**, 74 (2017).

[22] J. VandeVondele, M. Krack, F. Mohamed, M. Parrinello, T. Chassaing, and J. Hutter, Comput. Phys. Commun. **167**, 103 (2005).

[23] C. Adamo and V. Barone, J. Chem. Phys. **110**, 6158 (1999).

[24] S. Goedecker, M. Teter, and J. Hutter, Phys. Rev. B **54**, 1703 (1996).

[25] S. Grimme, J. Antony, S. Ehrlich, and H. Krieg, J. Chem. Phys. **132**, 154104 (2010).

[26] M. Guidon, J. Hutter, and J. VandeVondele, J. Chem. Theory Comput. **6**, 2348 (2010).

[27] G. Kresse and J. Furthmuller, Phys. Rev. B **54**, 11169 (1996).

[28] J. Klimes, D. R. Bowler, and A. Michaelides, Phys. Rev. B **83**, 195131 (2011).

[29] M. S. J. Barson, L. M. Oberg, L. P. McGuinness, A. Denisenko, N. B. Manson, J. Wrachtrup, and M. W. Doherty, Nano. Lett. **21**, 2962 (2021).

[30] W. A. Maza, V. M. Breslin, N. T. Plymale, P. A. DeSario, A. Epshteyn, J. C. Owrutsky, and B. B. Pate, Photochem. Photobiol. Sci. **18**, 1526 (2019).

[31] J. Mégrourèche, H. Bekerat, J. Y. Bian, A. Bui, J. Sankey, L. Childress, and S. A. Enger, Med. Phys. **50**, 7245 (2023).

[32] Z. P. Yang, F. Z. Shi, P. F. Wang, N. Raatz, R. Li, X. Qin, J. Meijer, C. K. Duan, C. Y. Ju, X. Kong, and J. F. Du, Phys. Rev. B **97**, 205438 (2018).

[33] L. M. Pham, S. J. DeVience, F. Casola, I. Lovchinsky, A. O. Sushkov, E. Bersin, J. Lee, E. Urbach, P. Cappellaro, H. Park, A. Yacoby, M. Lukin, and R. L. Walsworth, Phys. Rev. B **93**, 045425 (2016).

[34] S. Sangtawesin, B. L. Dwyer, S. Srinivasan, J. J. Allred, L. V. H. Rodgers, K. De Greve, A. Stacey, N. Dontschuk, K. M. O'Donnell, D. Hu, D. A. Evans, C. Jaye, D. A. Fischer, M. L. Markham, D. J. Twitchen, H. Park, M. D. Lukin, and N. P. de Leon, Phys. Rev. X **9**, 031052 (2019).

[35] J. P. Perdew, K. Burke, and M. Ernzerhof, Phys. Rev. Lett. **77**, 3865 (1996).

[36] Y. K. Zhang and W. T. Yang, Phys. Rev. Lett. **80**, 890 (1998).

[37] J. VandeVondele and J. Hutter, J. Chem. Phys. **127**, 114105 (2007).

[38] G. Bussi, D. Donadio, and M. Parrinello, J. Chem. Phys. **126**, 014101 (2007).

[39] B. Halle and G. Karlstrom, J. Chem. Soc., Faraday Trans. 1 **79**, 1047 (1983).

[40] P. Siyushev, M. Nesladek, E. Bourgeois, M. Gulka, J. Hruby, T. Yamamoto, M. Trupke, T. Teraji, J. Isoya, and F. Jelezko, Science **363**, 728 (2019).

[41] A. Lozovoi, H. Jayakumar, D. Daw, G. Vizkelethy, E. Bielejec, M. W. Doherty, J. Flick, and C. A. Meriles, National electronics review **4**, 717 (2021).

[42] D. Huang, S. Liu, I. Zeljkovic, J. F. Mitchell, and J. E. Hoffman, Rev. Sci. Instrum. **88**, 023705 (2017).

[43] S. J. Sque, R. Jones, and P. R. Briddon, Phys. Rev. B **73**, 085313 (2006).

[44] C. X. Li, X. Zhang, E. F. Oliveira, A. B. Puthirath, M. R. Neupane, J. D. Weil, A. G. Birdwell, T. G. Ivanov, S. Kong, T. Gray, H. Kannan, A. Biswas, R. Vajtai, D. S. Galvao, and P. M. Ajayan, Carbon **182**, 725 (2021).

[45] M. C. Salvadori, W. W. R. Araújo, F. S. Teixeira, M. Cattani, A. Pasquarelli, E. M. Oks, and I. G. Brown, Diam. Relat. Mater. **19**, 324 (2010).

[46] Y. S. Park, H. G. Son, D. H. Kim, H. G. Oh, D. S. Lee, M. H. Kim, K. M. Lim, and K. S. Song, Appl. Surf. Sci. **361**, 269 (2016).

[47] S. Y. Cui and E. L. Hu, Appl. Phys. Lett. **103**, 051603 (2013).

[48] C. J. Widmann, C. Giese, M. Wolfer, S. Kono, and C. E. Nebel, Phys. Status Solidi A **211**, 2328 (2014).

[49] D. S. Wastl, A. J. Weymouth, and F. J. Giessibl, Phys. Rev. B **87**, 245415 (2013).

[50] W. Melitz, J. Shen, A. C. Kummel, and S. Lee, Surf. Sci. Rep. **66**, 1 (2011).

[51] K. Bian, W. Zheng, X. Zeng, X. Chen, R. Stohr, A. Denisenko, S. Yang, J. Wrachtrup, and Y. Jiang, Nat. Commun. **12**, 2457 (2021).
[52] N. I. Hammer, J. W. Shin, J. M. Headrick, E. G. Diken, J. R. Roscioli, G. H. Weddle, and M. A. Johnson, Science **306**, 675 (2004).
[53] J. M. Herbert and M. P. Coons, Annu. Rev. Phys. Chem. **68**, 447 (2017).
[54] A. O. Sushkov, I. Lovchinsky, N. Chisholm, R. L. Walsworth, H. Park, and M. D. Lukin, Phys. Rev. Lett. **113**, 197601 (2014).
[55] F. F. de Oliveira, D. Antonov, Y. Wang, P. Neumann, S. A. Momenzadeh, T. Haussermann, A. Pasquarelli, A. Denisenko, and J. Wrachtrup, Nat. Commun. **8**, 15409 (2017).
[56] F. J. Giessibl, Rev. Sci. Instrum. **90**, 011101 (2019).
[57] K. Purckhauer, A. J. Weymouth, K. Pfeffer, L. Kullmann, E. Mulvihill, M. P. Krahn, D. J. Muller, and F. J. Giessibl, Sci. Rep. **8**, 9330 (2018).
[58] W. T. Zheng, K. Bian, X. K. Chen, Y. Shen, S. C. Zhang, R. Stohr, A. Denisenko, J. Wrachtrup, S. Yang, and Y. Jiang, Nat. Phys. **18**, 1317 (2022).
[59] K. J. Lee, N. Elgrishi, B. Kandemir, and J. L. Dempsey, Nat. Rev. Chem. **1**, 0039 (2017).
[60] P. Deak, B. Aradi, M. Kaviani, T. Frauenheim, and A. Gali, Phys. Rev. B **89**, 079905 (2014).
[61] M. V. Hauf, B. Grotz, B. Naydenov, M. Dankerl, S. Pezzagna, J. Meijer, F. Jelezko, J. Wrachtrup, M. Stutzmann, F. Reinhard, and J. A. Garrido, Phys. Rev. B **83**, 081304(R) (2011).
[62] D. Zhu, L. H. Zhang, R. E. Ruther, and R. J. Hamers, Nat. Mater. **12**, 836 (2013).
[63] G. V. Buxton, C. L. Greenstock, W. P. Helman, and A. B. Ross, J. Phys. Chem. Ref. Data **17**, 513 (1988).
[64] P. E. Mason, H. C. Schewe, T. Buttersack, V. Kostal, M. Vitek, R. S. McMullen, H. Ali, F. Trinter, C. Lee, D. M. Neumark, S. Thurmer, R. Seidel, B. Winter, S. E. Bradforth, and P. Jungwirth, Nature (London) **595**, 673 (2021).
[65] J. K. Lee, K. L. Walker, H. S. Han, J. Kang, F. B. Prinz, R. M. Waymouth, H. G. Nam, and R. N. Zare, Proc. Natl. Acad. Sci. U.S.A. **116**, 19294 (2019).
[66] H. X. Hao, I. Leven, and T. Head-Gordon, Nat. Commun. **13**, 280 (2022).
[67] J. Tisler, T. Oeckinghaus, R. J. Stöhr, R. Kolesov, R. Reuter, F. Reinhard, and J. Wrachtrup, Nano Lett. **13**, 3152 (2013).
[68] M. S. Grinolds, M. Warner, K. De Greve, Y. Dovzhenko, L. Thiel, R. L. Walsworth, S. Hong, P. Maletinsky, and A. Yacoby, Nat. Nanotechnol. **9**, 279 (2014).
[69] T. Fukuma, Y. Ueda, S. Yoshioka, and H. Asakawa, Phys. Rev. Lett. **104**, 016101 (2010).
[70] A. Laraoui, F. Dolde, C. Burk, F. Reinhard, J. Wrachtrup, and C. A. Meriles, Nat. Commun. **4**, 1651 (2013).
[71] T. Staudacher, N. Raatz, S. Pezzagna, J. Meijer, F. Reinhard, C. A. Meriles, and J. Wrachtrup, Nat. Commun. **6**, 8527 (2015).
[72] A. Afrough, Eur. Phys. J. E **44**, 107 (2021).
[73] I. Schulthess, A. Fratangelo, P. Hautle, P. Heil, G. Markaj, M. Persoz, C. Pistillo, J. Thorne, and F. M. Piegsa, J. Magn. Reson. **353**, 107496 (2023).
[74] L. P. McGuinness, L. T. Hall, A. Stacey, D. A. Simpson, C. D. Hill, J. H. Cole, K. Ganesan, B. C. Gibson, S. Prawer, P. Mulvaney, F. Jelezko, J. Wrachtrup, R. E. Scholten, and L. C. L. Hollenberg, New J. Phys. **15**, 073042 (2013).
[75] M. Holz, S. R. Heil, and A. Sacco, Phys. Chem. Chem. Phys. **2**, 4740 (2000).
[76] M. Chen, L. X. Zheng, B. Santra, H. Y. Ko, R. A. DiStasio, M. L. Klein, R. Car, and X. F. Wu, Nat. Chem. **10**, 413 (2018).